

# Properties of the Two-Dimensional Electron Gas Close to the Fermi-Liquid Quantum Critical Point

M. Baldo,<sup>1</sup> V. V. Borisov,<sup>2</sup> J. W. Clark,<sup>3</sup> V. A. Khodel,<sup>2</sup> and M. V. Zverev<sup>2</sup>

<sup>1</sup>*Istituto Nazionale di Fisica Nucleare, Sezione di Catania,  
I-95123, Catania, Italy*

<sup>2</sup>*Russian Research Center Kurchatov Institute,  
Moscow, 123182 Russia*

<sup>3</sup>*McDonnell Center for the Space Science and Department of Physics,  
Washington University, St.Louis, MO 63130, USA*

(Dated: November 15, 2018)

The rearrangement of single-particle degrees of freedom of a dilute two-dimensional electron gas in the vicinity of the quantum critical point is examined within a microscopic approach. It is shown that just beyond the critical point, the Landau state undergoes self-consistent rearrangement of the quasiparticle spectrum and momentum distribution. At very low temperatures, there emerges a multi-connected quasiparticle momentum distribution. With increasing temperature, two crossovers occur: a fermion condensate appears in the first and disappears in the second, giving way to universal non-Fermi-liquid behavior. Manifestations of these crossovers in thermodynamic properties of the electron gas are studied and characterized. The four quasiparticle phases predicted to exist in the vicinity of the critical point are collected in a schematic phase diagram.

PACS numbers: 71.10.Hf, 71.27.+a, 71.10.Ay

## I. INTRODUCTION

The two-dimensional (2D) electron gas is a widely used physical model for the electron system of the inversion layer in high-quality Si-MOS devices. The density of that system can be varied over several order of magnitude upon varying the external electric field orthogonal to the layer. The potential energy of the 2D electron gas is proportional to the inverse of the average distance between electrons, while its kinetic energy is proportional to the inverse square of this distance. Thus, with *decreasing* density, the electron gas passes from a regime of weak correlations to one of strong correlations. Although experimental study of the 2D electron gas began almost 40 years ago,<sup>1</sup> it is only recently that experiments<sup>2,3</sup> have reached a degree of accuracy such that the explosive growth of the effective mass  $M^*$  of Landau quasiparticles is observed as the density approaches a critical value  $\rho_\infty \simeq 8 \times 10^{10} \text{ cm}^{-2}$ . Evidence for divergence of the quasiparticle effective mass is also found in 2D liquid <sup>3</sup>He (see Refs. 4,5,6) and in some heavy-fermion materials.<sup>7,8,9,10,11,12</sup> At zero temperature, the point  $x = x_\infty$  of an external parameter  $x$  (density, pressure, magnetic field) at which the effective mass is predicted or found to diverge is known as the quantum critical point (QCP).<sup>7,11,13</sup> Properties of strongly correlated Fermi system in the vicinity of the QCP exhibit non-Fermi liquid (NFL) behavior, i.e. they cannot be described within the Landau FL theory, as ordinarily interpreted. It is often supposed (see e.g. Refs. 14,15,16) that the collective degrees of freedom are the *dramatis personae* near the QCP; indeed, that they are responsible for the occurrence of the QCP itself and for the properties of the system in its vicinity. We follow a different strategy, exploring instead the possibility that the

single-particle (sp) degrees of freedom are the main characters of the drama. In this paper, we will show that the QCP is inherent in Landau FL theory, and that a tool exists *within* this theory for describing the system in the immediate vicinity of the QCP and on *both* sides of it.

We focus on the 2D electron gas, for which a microscopic, *ab initio* non-perturbative approach was developed in Refs. 18,19,20. Applying this method, it was found that at  $T = 0$  the effective mass  $M^*$  of the 2D electron gas diverges as the dimensionless parameter  $r_s = \sqrt{2}Me^2/p_F$  (where  $p_F$  is the Fermi momentum) approaches a critical value  $r_s^\infty \simeq 7$ . This result for the critical spacing parameter  $r_s$  is in reasonable agreement with the experimental value  $\simeq 8 - 9$  cited in Refs. 2,22.

Fig. 1 presents results<sup>20</sup> of evaluation of the single-particle energy  $\epsilon(p)$  (measured from the chemical potential  $\mu$ ), for the 2D electron gas at a set of  $r_s$  values near the critical point  $r_s^\infty$ . As seen in this figure, the spectrum acquires an inflection point at the critical dilution, i.e.,  $\epsilon(p, r_s^\infty) \propto (p - p_F)^3$ , a situation first analyzed in Ref. 21. Beyond this point, meaning  $r_s > r_s^\infty$ , the conventional Landau state, characterized at zero temperature by a Fermi-step quasiparticle momentum distribution  $n_{\text{FL}}(p) = \theta(p_F - p)$ , becomes unstable against spontaneous creation of quasiparticle-quasihole pairs. We call attention here to the fact that at  $T = 0$  a necessary condition for stability of the conventional Landau state is positivity of the variation of the ground-state energy with respect to any admissible variation of the quasiparticle momentum distribution from  $n_{\text{FL}}(p)$ . More explicitly, it is necessary that

$$\delta E = \int \epsilon(p, [n]) \delta n(p) dv > 0 \quad (1)$$

holds for  $n(p) = n_{\text{FL}}(p)$  and variations satisfying the

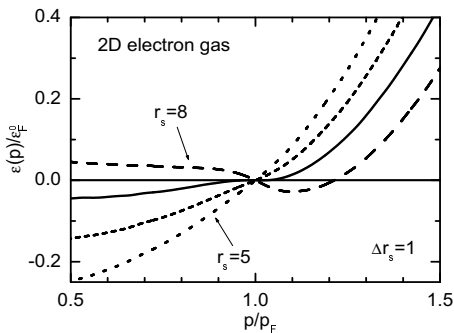


FIG. 1: Single-particle spectrum  $\epsilon(p)$  of the homogeneous two-dimensional electron gas in units of  $\epsilon_F^0 = p_F^2/2M$ , evaluated at  $T = 0$  for different values of  $r_s$ .

particle-number constraint

$$\int \delta n(p) dv = 0, \quad (2)$$

where  $dv = 2d^2p/(2\pi)^2$ . This stability condition (1) is met by  $n_{\text{FL}}$  provided the corresponding spectrum  $\epsilon(p)$  has a single zero at  $p = p_F$ . But as seen from Fig. 1, just beyond the critical point  $r_s^\infty$  the spectrum takes on a cubic-like behavior with *three* zeros near the Fermi surface. (It is worth noting that a similar shape for the single-particle spectrum of 2D liquid  $^3\text{He}$  has been found in the microscopic calculation of Ref. 23 based on the method of correlated basis functions<sup>24,25</sup> (CBF).) According to Eq. (1), a spectrum  $\epsilon(p)$  having this shape implies that one can lower the energy of the system by introducing a quasihole at a certain momentum  $p < p_F$  for which  $\epsilon(p) < 0$ , and a quasiparticle at a certain momentum  $p > p_F$  for which  $\epsilon(p) > 0$ .

In the general framework of Landau theory, the quasiparticle spectrum is a functional

$$\epsilon(p, [n]) = \frac{\delta E}{\delta n(p)} - \mu \quad (3)$$

of the quasiparticle momentum distribution  $n(p)$ ; hence the two quantities should be evaluated self-consistently. The functional approach as formulated and applied in Refs. 18,19,20 cannot be used in the 2D electron gas beyond the critical point  $r_s^\infty$ , since this approach has so far only been developed for states of Fermi systems describable in terms of standard Landau quasiparticles having the Fermi-step momentum distribution  $n_{\text{FL}}(p)$ . Moreover, extension of this approach to finite temperatures remains incomplete.

Nevertheless, an effective tool is available for self-consistent evaluation of the single-particle spectrum  $\epsilon(p)$  and momentum distribution  $n(p)$  beyond the point of instability of conventional Landau state, and indeed within Landau theory itself. This tool is the basic Landau formula

$$\frac{\partial \epsilon(p)}{\partial \mathbf{p}} = \frac{\mathbf{p}}{M} + \int f(\mathbf{p}, \mathbf{p}') \frac{\partial n(p')}{\partial \mathbf{p}'} dv' \quad (4)$$

relating the group velocity of quasiparticles,  $\partial \epsilon / \partial \mathbf{p}$ , to their momentum distribution

$$n(p) = \frac{1}{1 + e^{\epsilon(p)/T}} \quad (k_B = 1), \quad (5)$$

in terms of the Landau interaction function  $f(\mathbf{p}, \mathbf{p}')$ . The quasiparticle interaction function is the second variational derivative of the energy functional  $E[n]$ ,

$$f(\mathbf{p}, \mathbf{p}', [n]) = \frac{\delta^2 E}{\delta n(\mathbf{p}) \delta n(\mathbf{p}')}, \quad (6)$$

and hence itself depends on the quasiparticle momentum distribution  $n(p)$ . If non-zero temperatures are considered, the  $T$ -dependence of this function should in principle also be taken into account. The theory presented here rests on two main assumptions. The first is that the difference between the interaction  $f(\mathbf{p}, \mathbf{p}', r_s, [n])$  corresponding to the *true* quasiparticle distribution  $n(p)$  at  $r_s > r_s^\infty$ , and its counterpart  $f(\mathbf{p}, \mathbf{p}', r_s, [n_{\text{FL}}])$  evaluated with Landau distribution  $n_{\text{FL}}(p)$ , is small as long as the relative size of the region of momentum space in which  $n_{\text{FL}}(p)$  is altered, remains small. Thus, we restrict our analysis to values of  $r_s$  adjacent to the QCP. The second assumption is that the  $T$ -dependent terms in the quasiparticle interaction function produce contributions to the single-particle spectrum of order of  $T/\epsilon_F^0$ , where  $\epsilon_F^0 = p_F^2/2M$ . Thus, our analysis is further restricted to the regime of very low temperatures  $T/\epsilon_F^0 \ll 1$ . These two assumptions allow us to use the quasiparticle interaction function obtained from the functional approach in the Landau relation (4), which becomes an equation for self-consistent evaluation of the quasiparticle spectrum and the quasiparticle momentum distribution.

In Sec. II, we outline the approximation method employed for evaluation of the quasiparticle interaction function of the 2D electron gas and the self-consistent scheme for subsequent calculation of  $\epsilon(p)$  and  $n(p)$ . Working within this framework, we then explore scenarios for rearrangement of single-particle degrees of freedom of the system just beyond its QCP (Sec. III). Section IV is devoted to calculation and analysis of the corresponding thermodynamic properties of the 2D electron gas near the QCP. In Section V, the quasiparticle phase diagram of the system is constructed and discussed. An Appendix presents further details on the calculation of the quasiparticle interaction function.

## II. SINGLE-PARTICLE SPECTRUM AND QUASIPARTICLE INTERACTION FUNCTION

The well-known Feynman-Hellman formula, written as

$$E = \tau - \frac{1}{2} \int_0^{\epsilon^2} de^2 \int dq \int_0^\infty \frac{d\omega}{\pi} [\text{Im} \chi(q, \omega) + \pi \rho \delta(\omega)] \quad (7)$$

for the 2D electron gas, relates the energy  $E$  of the system to its response function  $\chi(q, \omega)$ . This relation enables one

to evaluate both the single-particle spectrum at  $T = 0$ , by calculating the first derivative of Eq. (7) as in Ref. 20, and the quasiparticle interaction function, as described herein. The latter is given by

$$f(\mathbf{p}, \mathbf{p}') = -\frac{1}{2} \int_0^{\epsilon^2} de^2 \int \frac{d^2 q}{2\pi q} \int_0^\infty \frac{d\omega}{\pi} \text{Im} \left[ \frac{\delta^2 \chi(\mathbf{q}, \omega)}{\delta n(\mathbf{p}) \delta n(\mathbf{p}')} \right] \quad (8)$$

in term of the second derivative of  $\chi(\mathbf{q}, \omega)$  with respect to the occupation numbers.

If the Landau quasiparticle interaction function is available, Eq. (4) can be treated as an equation for  $n(p)$ . Specifically, making use of Eq. (5) the Landau relation can be recast in the form

$$-\frac{T}{n(p)[1-n(p)]} \frac{\partial n(p)}{\partial \mathbf{p}} = \frac{\mathbf{p}}{M} + \int f(\mathbf{p}, \mathbf{p}') \frac{\partial n(p')}{\partial \mathbf{p}'} dv' , \quad (9)$$

with  $n(p) = -\int_p^\infty (dn(p')/dp') dp'$ .

A microscopic prescription for evaluation of the quasiparticle interaction function is given in the Appendix. Although full numerical realization of this scheme presents a formidable challenge, calculation of harmonics of the interaction function is tractable. Based on analysis of different contributions to  $f(\mathbf{p}, \mathbf{p}', r_s, [n_{\text{FL}}])$  and computation of its zeroth and first harmonics at the Fermi surface as functions of  $r_s$ , we have developed a method for approximate determination of the quasiparticle interaction function. To elucidate the essence of this approximation, we note first that if the momenta  $\mathbf{p}$  and  $\mathbf{p}'$  lie exactly at the Fermi surface, the interaction function depends only on the difference  $q = |\mathbf{p} - \mathbf{p}'|$ . Analysis has shown that the main contribution to this function has a strongly pronounced peak at  $q_0 \simeq 1.97 p_F$ . Since our considerations are restricted to the immediate vicinity of the QCP, only momenta  $p$  and  $p'$  close to  $p_F$  enter Eq. (9). Accordingly, we approximate  $F(\mathbf{p}, \mathbf{p}') = N_0 f(\mathbf{p}, \mathbf{p}')$ , where  $N_0 = M/\pi$ , in terms of the analytical form

$$F(q) = -\frac{\gamma(r_s)}{(q^2/q_0^2 - 1)^2 + \beta^2}, \quad (10)$$

which by construction is peaked at  $q_0$ . To choose the other parameters specifying this function, we have made *ab initio* calculations of the zeroth and first harmonics of the interaction function and their derivatives with respect to  $r_s$ , and used the results, namely  $F_0(r_s^\infty) = -1.3$ ,  $F_1(r_s^\infty) = 1.0$ , and  $(r_s^\infty/F_1(r_s^\infty))dF_1/dr_s = 1.05$ , as data to be fit by adjusting  $\gamma$  and  $\beta$  in Eq. (10). In this way these parameters were determined to be  $\gamma(r_s) = 0.08(1 + 1.05 r_s/r_s^\infty)$  and  $\beta = 0.135$ .

With the interaction function dependent only on  $|\mathbf{p} - \mathbf{p}'|$ , Eq. (4) reduces to the relation

$$\epsilon(p) = \epsilon_0(p) + \int f(|\mathbf{p} - \mathbf{p}'|) n(p') dv' , \quad (11)$$

in which  $\epsilon_0(p) = p^2/2M - \mu$  is the bare sp spectrum. Eq. (11), together with Eq. (5) and the normalization

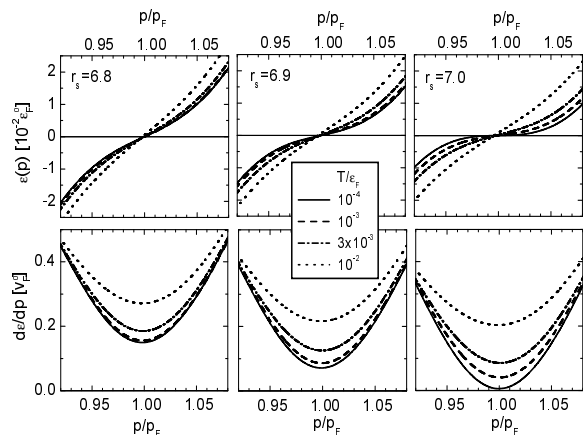


FIG. 2: Single-particle spectrum  $\epsilon(p)$  in units of  $10^{-2} \epsilon_F^0$  (top panels) and derivative  $d\epsilon(p)/dp$  in units of  $v_F^0 = p_F/M$  (bottom panels) for the 2D electron gas at  $r_s = 6.8$  (left column),  $r_s = 6.9$  (middle column), and  $r_s = 7.0$  (right column). The spectrum and its derivative are shown as functions of  $p/p_F$  at four (line-coded) temperatures expressed in units of  $\epsilon_F^0$ .

condition

$$\int n(p) dv = \rho, \quad (12)$$

provide a set of equations for self-consistent evaluation of the quasiparticle spectrum  $\epsilon(p)$  and momentum distribution  $n(p)$ . The chemical potential  $\mu$ , which enters Eq. (11) as a constant of integration, is also determined self-consistently.

### III. REARRANGEMENT OF SINGLE-PARTICLE DEGREES OF FREEDOM

We have solved Eq. (11) for  $r_s$  values situated in the vicinity of  $r_s^\infty$  and on both sides of the QCP. To analyze the nature of the solutions, we start with the results shown in Fig. 2 at  $r_s < r_s^\infty$ , i.e., for densities above that of the QCP. As seen in the bottom panels of this figure, where the derivative  $d\epsilon/dp$  is plotted against momentum  $p$ , the effective mass grows rapidly as  $r_s$  approaches the QCP. The ratio  $M^*/M$  at low temperature is about 6 at  $r_s = 6.8$ , reaches 15 at  $r_s = 6.9$ , and diverges at  $r_s = 7.0$ . We observe that near the QCP, the effective mass  $M^*(r_s)$  decreases with increasing temperature, and the closer  $r_s$  is to  $r_s^\infty$ , the more pronounced is the decrease of  $M^*(T)$ . The results shown in the bottom-right panel of Fig. 2 are in accord with the behavior of the group velocity predicted by the inflection-point model of the QCP proposed in Ref. 21, in that  $p_F/M^*(T)$  is found to vary approximately as  $T^{2/3}$ .

Results from evaluation of the quasiparticle momentum distribution  $n(p)$  and spectrum  $\epsilon(p)$  at  $r_s > r_s^\infty$ , i.e., for densities below that of the QCP, are displayed in Figs. 3 and 4. Inspection of Fig. 3 informs us that at low temperatures in this region beyond the critical point, the

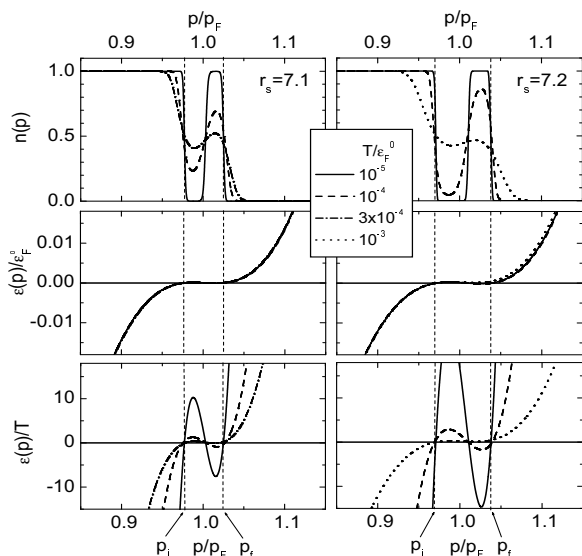


FIG. 3: Occupation number  $n(p)$  (top panels), single-particle spectrum  $\epsilon(p)$  in units of  $\epsilon_F^0$  (middle panels), and ratio  $\epsilon(p)/T$  (bottom panels) for the 2D electron gas at  $r_s = 7.1$  (left column) and  $r_s = 7.2$  (right column). All three quantities are shown as functions of  $p/p_F$  at different temperatures expressed in units of  $\epsilon_F^0$ .

quasiparticle degrees of freedom are rearranged in a scenario involving the formation of a multi-connected Fermi surface. To the authors' knowledge, Fröhlich<sup>31</sup> was the first to call attention to the possibility of this type of Fermi surface (see also Ref. 32). At  $r_s = 7.1$  and  $r_s = 7.2$ , the rearranged quasiparticle momentum distribution of the 2D electron gas at  $T = 0$ , for either spin projection, is defined by a fully occupied circle ( $n(p) = 1$ ), surrounded by an empty inner ring ( $n(p) = 0$ ), surrounded in turn by a fully occupied outer ring, all centered on  $p = 0$ . At the small finite temperatures indicated in Fig. 3, increasing  $T$  leads to population of the inner ring ( $n(p) > 0$ ) at the expense of depletion of the outer ring ( $n(p) < 1$ ). The spectrum appears to have a cubic shape

$$\epsilon(p) \simeq D(r_s) \frac{p_F(p - p_F)}{M} + \lambda \frac{(p - p_F)^3}{Mp_F}, \quad (13)$$

with three zeroes. In this expression, the coefficient  $D(r_s)$ , being negative beyond the QCP, vanishes at  $r_s = r_s^\infty$ , while the coefficient  $\lambda$  of the cubic term does not depend on  $r_s$ . As the system moves away from the QCP at  $r_s > r_s^\infty$ , the relative size of the momentum region affected by the quasiparticle rearrangement, measured by  $\eta = (p_f - p_i)/p_F$ , increases as  $\eta \propto (r_s/r_s^\infty - 1)^{1/2}$ . With rising temperature, the momentum distribution  $n(p, T)$  and the ratio  $\epsilon(p, T)/T$  change dramatically. At  $T/\epsilon_F^0 \sim 3 \times 10^{-4}$  (for  $r_s = 7.1$ ) and  $T/\epsilon_F^0 \sim 10^{-3}$  (for  $r_s = 7.2$ ) the values of  $n(p)$  in inner and outer rings of the  $T = 0$  distribution equalize, and the extrema in the spectrum  $\epsilon(p)$  disappear.

As the temperature continues to increase, the quasi-

particle spectrum and the momentum distribution each undergo a metamorphosis illustrated in Fig. 4. Inspection of the temperature dependence of these quantities reveals a crossover from a state having a multi-connected momentum distribution created by formation of a ring-shaped “bubble,” to a state characterized by a region of momentum space in which the ratio  $\epsilon(p, T)/T$  and the distribution  $n(p)$  are independent of temperature. The existence of such a finite domain over which temperature independence prevails is a signature of the phenomenon of fermion condensation, i.e., the formation of a fermion condensate (FC) in the momentum region involved.<sup>19,34</sup> Comparing Figs. 3 and 4, it is seen that the size and location of the region of momentum space occupied by the FC coincide respectively with the size and location of the region in which the “bubble” rearrangement scenario – depopulation of the inner ring and population of the outer ring – operates at lower temperatures.

The emergence, at low but not the lowest temperatures, of a sizeable domain in momentum space within which the occupation numbers differ from 1 and 0, implies that there is a crossover from a state with small entropy to another state with sufficiently large entropy. To some extent the phenomenon that occurs is analogous the Kosterlitz-Thouless transition.<sup>35</sup> Although we are dealing with a crossover rather than a real phase transition, this analogy enables us to estimate the temperature of the crossover. To do so, we compare the free energies per particle  $F = E - TS$  in the bubble phase and the FC phase. The entropy associated with the bubble rearrangement is taken to be zero, while that corresponding to the FC is estimated as  $\eta = (p_f - p_i)/p_F$ . The loss in energy due to the transition from the bubble phase to the FC phase is estimated<sup>36</sup> as  $\Delta E \sim |D(r_s)| \eta^2 \epsilon_F^0$ , and the coefficient of the linear term in Eq. (13), as  $|D(r_s)| \sim \eta^2$ . Thus,  $\Delta E \sim \eta^4 \epsilon_F^0$ . Since the difference  $\Delta S$  is of order  $\eta$ , the free energy of the FC state becomes lower than that of the bubble state at  $T_0 \sim \Delta E/\Delta S \sim |D(r_s)| \eta \epsilon_F^0 \sim |D(r_s)|^{3/2} \epsilon_F^0$ .

Proceeding to higher temperatures, the region belonging to the FC gradually shrinks and finally disappears. To analyze the type of crossover taking place in this case, it is useful to study thermodynamic characteristics of the 2D electron gas.

#### IV. LOW-TEMPERATURE THERMODYNAMIC PROPERTIES OF 2D ELECTRON GAS

The density of states

$$N(T) = - \int \frac{dn(\epsilon)}{d\epsilon} d\epsilon \quad (14)$$

is a property well suited for analysis of the behavior of the 2D electron gas in different temperature regimes. The ratio of the inverse of this quantity to its inverse for the corresponding 2D Fermi gas,  $N_0^{-1} = \pi/M$ , is plotted

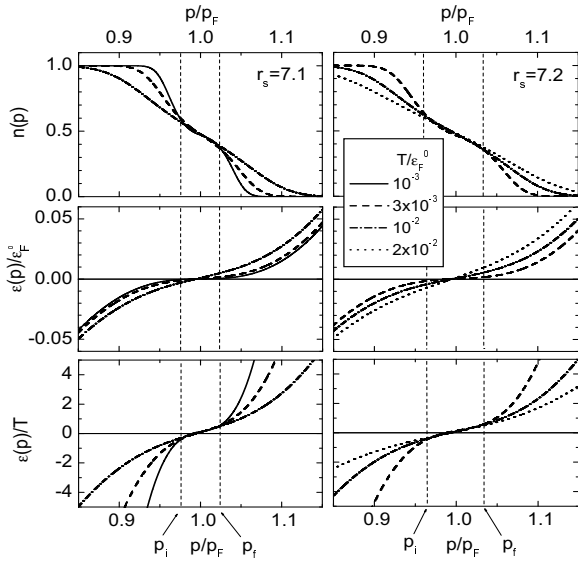


FIG. 4: Same as in Fig. 3 but at higher temperatures.

on a log-log scale in Fig. 5. The horizontal line corresponds to FL behavior, while the straight line with slope (or critical index)  $\alpha$  corresponds to the NFL regime with  $N(T) \propto T^{-\alpha}$ . As seen in the top panel of Fig. 5, the FL behavior of the density of states at  $r_s < r_s^\infty$  persists only up to some characteristic temperature  $T^*$ . In the region around  $T^*$ , a crossover occurs from FL to NFL behavior, with a critical index  $\alpha \simeq 0.6$ . This result is in essential agreement with the inflection-point model of the QCP developed in Ref. 21, which yields  $\alpha = 2/3$ . The difference between 0.6 and  $2/3$  could be due to the term in the sp spectrum quadratic in  $p - p_F$ , which is absent in the inflection-point model.<sup>21</sup> According to the top panel of Fig. 5,  $T^* \sim 10^{-3}\epsilon_F^0$  at  $r_s = 6.8$ . As  $r_s$  approaches the point  $r_s^\infty = 7.0$ , the temperature  $T^*$  decreases and vanishes at the QCP. This is apparent in the middle panel of Fig. 5: at  $r_s = 7.0$  the inverse of the density of states,  $N^{-1}(T)$ , shows universal NFL behavior with a critical index  $\alpha \simeq 0.6$  within the entire range of temperatures under consideration. As demonstrated in the bottom panel of this figure, at  $r_s > r_s^\infty$  the quantity  $N^{-1}(T)$  undergoes two crossovers separating three different temperature regimes. At low temperatures, it exhibits FL behavior with a large effective mass. In the vicinity of  $T_0$  (which is roughly  $10^{-4}\epsilon_F^0$  at  $r_s = 7.2$ ), a crossover occurs from the FL regime to an intermediate NFL regime. With further increase of temperature, another crossover occurs in the vicinity of  $T^*$  (which is roughly  $5 \times 10^{-3}\epsilon_F^0$  at  $r_s = 7.2$ ), leading to the NFL regime with critical index  $\alpha \simeq 0.6$ .

Returning to Figs. 3 and 4, we may clarify the relationship of the three temperature regimes exhibited by the density of states, to the different regimes of behavior found in the quasiparticle momentum distribution  $n(p)$  and spectrum  $\epsilon(p)$ . The bubble phase, with its cubic-like spectrum (13), evidently corresponds to the FL behav-

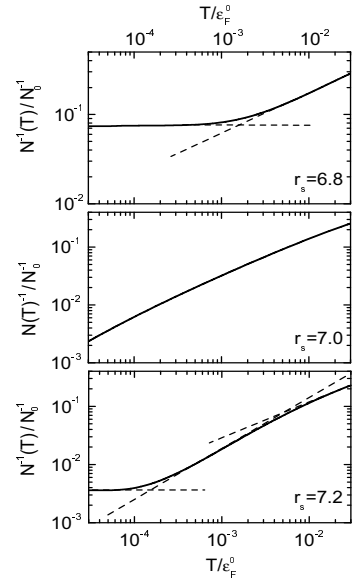


FIG. 5: Inverse of density of states  $N^{-1}(T)$  in units of  $N_0^{-1}$  for the 2D electron gas at  $r_s = 6.8$  (top panel),  $r_s = 7.0$  (middle panel), and  $r_s = 7.2$  (bottom panel). Dashed lines show different temperature regimes.

ior of  $N^{-1}(T)$ . Smoothing of the bubble and flattening of the quasiparticle spectrum  $\epsilon(p)$  in the region  $[p_i, p_f]$  corresponds to the crossover to the FC state. However, the spectrum  $\epsilon(p)$  is also flat in the regions adjacent to the points  $p_i$  and  $p_f$ , and hence these regions also play a significant role in producing NFL behavior of thermodynamic properties. Indeed, the density of states,

$$N(T) \equiv \frac{N_0 [\nu_f(T) + \nu_n(T)]}{T}, \quad (15)$$

decomposes into a sum of the FC term

$$\nu_f(T) = \frac{1}{p_F} \int_{p_i}^{p_f} n_*(p) [1 - n_*(p)] dp \sim \eta \quad (16)$$

and non-condensate part

$$\nu_n(T) \equiv \nu_n^>(T) + \nu_n^<(T) \quad (17)$$

consisting of two terms. Upon introducing

$$\nu_n(T; \epsilon_1, \epsilon_2) = \frac{1}{p_F} \int_{\epsilon_1}^{\epsilon_2} \frac{n(\epsilon) [1 - n(\epsilon)] d\epsilon}{(d\epsilon/dp)}, \quad (18)$$

one can rewrite these two terms as  $\nu_n^< = \nu_n(T; -\mu, \epsilon_i)$  and  $\nu_n^> = \nu_n(T; \epsilon_f, \infty)$ . At  $\eta \ll 1$  the group velocity near the boundary  $p_f$  can be approximated using

$$d\epsilon(p \rightarrow p_f)/dp = v_f(T) + v^{(2)}(p - p_f)^2 + \dots \quad (19)$$

To estimate the value of  $v_f(T)$ , i.e. the slope of the FC “plateau” in the spectrum  $\epsilon(p)$ , we substitute the

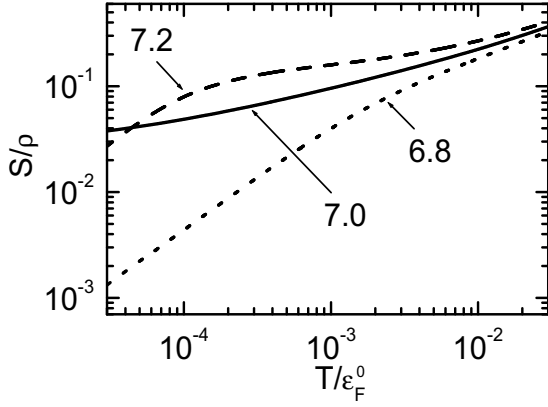


FIG. 6: Entropy per electron for the 2D electron gas as a function of temperature in units of  $\varepsilon_F^0$  at three values of  $r_s$ .

momentum-independent result  $n_*(p)$  for the momentum distribution in the region  $[p_i, p_f]$  into the Fermi-Dirac formula (5) and obtain

$$\epsilon(p, T \geq T_0) = T \ln \frac{1 - n_*(p)}{n_*(p)}, \quad p_i < p < p_f. \quad (20)$$

As seen in the bottom panels of Fig. 4, the width  $\epsilon(p_f) - \epsilon(p_i) \equiv \epsilon_f - \epsilon_i$  of the FC zone at  $T > T_0$  appears to be of order  $T$  and almost independent of  $\eta$  for  $\eta_{\min} \sim 10^{-2}$ . Thus, at  $\eta > \eta_{\min}$  the FC group velocity is estimated as

$$\left( \frac{d\epsilon(p)}{dp} \right)_T \sim \frac{T}{\eta p_F}, \quad p_i < p < p_f, \quad (21)$$

which in turn yields  $v_f(T) \sim T$ . The formula for the group velocity outside the FC region but near the point  $p_i$  is analogous to (19) with  $v_i(T) \sim T$ . Using these results in algebraic manipulations similar to those performed in Ref. 21, we arrive at the relation

$$N(T) = N_0 \tau^{-1} [\nu_f + \nu_n \tau^{1/3}] + \text{const.}, \quad (22)$$

expressed in terms of the dimensionless temperature  $\tau = T/\varepsilon_F^0$ .

The FC is seen to play an insignificant role at small  $\eta$ , say  $\eta < \tau^{1/3}$ , where the density of states behaves as

$$N(T) \propto T^{-2/3}. \quad (23)$$

In the opposite case,  $\eta > \tau^{1/3}$ , the FC contribution dominates in Eq. (22). In our calculation, the intermediate situation  $\eta \sim \tau^{1/3}$  occurs, so the behavior of the density of states in the region  $T_0 < T < T^*$  corresponds to a superposition of two terms in Eq. (22) of the same order.

The NFL difference  $\Delta\chi(T, \rho) = \chi(T, \rho) - \chi_{\text{FL}}(\rho)$  between the magnetic susceptibility and Pauli susceptibility is determined as

$$\Delta\chi(T, \rho) \sim \mu_B^2 N_0 \tau^{-1} \frac{\nu_f + \nu_n \tau^{1/3}}{1 + G_0}, \quad (24)$$

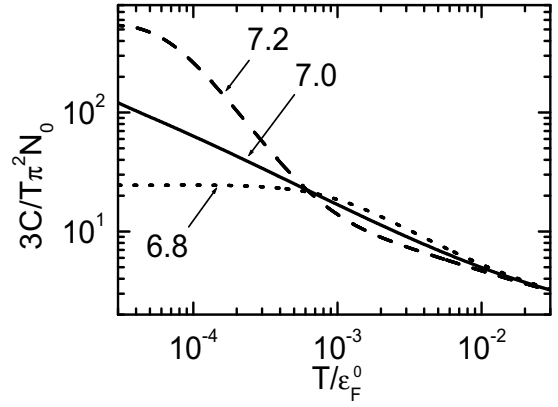


FIG. 7: Ratio  $3C/T\pi^2N_0$  for 2D electron gas at three values of the parameter  $r_s$  is shown against temperature  $T$  in units of  $\varepsilon_F^0$ .

where  $G_0$ , the zeroth harmonic of the spin-spin quasiparticle interaction function, is independent of density in advance of the QCP.<sup>2</sup> The following behaviors of the magnetic susceptibility derive from the above findings for the density of states. At  $\tau > \tau^* \propto \eta^3$ , one has

$$\chi(T) \propto T^{-2/3}, \quad (25)$$

whereas at  $\tau < \tau^*$  the magnetic susceptibility of the 2D electron gas,

$$\chi(T) \propto T^{-1}, \quad (26)$$

imitates that of a gas of localized spins. At  $\tau < \tau_0 < \tau^*$  the Curie-like behavior (26) is replaced by independence of  $T$ .

Fig. 6 shows the entropy per electron on a log-log scale at three values of  $r_s$ . Three different regimes may be discerned. Two of them are seen below the QCP, specifically at  $r_s = 6.8$ , namely (i) the FL domain with the usual linear temperature dependence and (ii) the NFL regime where  $S(T) \propto T^{1-\alpha}$  with  $\alpha \simeq 0.6$ . At the critical point, i.e., at  $r_s = 7.0$ , the slope of the curve  $S(T)$  is almost independent of temperature. Beyond the QCP, i.e., for  $r_s > 7.0$ , all three regimes are present, (i) the FL regime at low  $T$ , (ii) the intermediate NFL regime corresponding the emergence of the FC, and (iii) the NFL regime with  $\alpha \simeq 0.6$ . Similar observations follow from analysis of Fig. 7, where the ratio  $C(T)/T$  of the specific heat to temperature is depicted. The sharp drop of this ratio at  $r_s = 7.2$  corresponds to the crossover to the FC state, where the temperature dependence of the entropy is weak.

The evolution of the temperature regimes with passage through the critical point are clearly revealed when the reduced Sommerfield-Wilson ratio

$$R_{\text{SW}}^{(0)}(T) = \frac{\pi^2 \chi_0(T) T}{3\mu_B^2 C(T)}, \quad (27)$$

where  $\chi_0(T) = (1 + G_0)\chi(T)$ , is plotted against temperature for different  $r_s$  values in the critical region. This

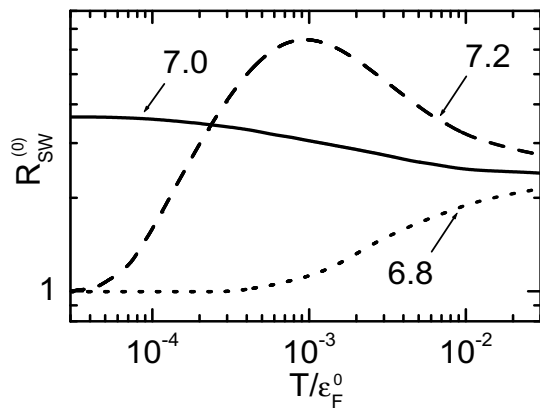


FIG. 8: Temperature dependence of the Sommerfeld-Wilson ratio  $R_{\text{SW}}^{(0)} = \pi^2 T \chi_0(T) / 3\mu_B^2 C(T)$  for the 2D electron gas in units of  $\epsilon_F^0$ , plotted for three values of the radius parameter  $r_s$ .

quantity is unity for the FL, and is usually strongly enhanced in case of NFL behavior.<sup>37</sup> At  $r_s = 6.8$ , the crossover from FL to NFL behavior is reflected in an enhancement of  $R_{\text{SW}}^{(0)}(T)$  for  $T > 10^3 \epsilon_F^0$ . At  $r_s = 7.2$ , the ratio (27) goes to unity in the low-temperature limit, confirming the FL character of the bubble phase, whereas its enhancement to a value  $\sim 7$  and subsequent decrease to  $\sim 3$  with increasing temperature reflect the two crossovers discussed above.

Up to this point, we have changed temperature at fixed values of  $r_s$ . Let us now go across the critical value  $r_s^\infty$  at fixed temperature. The results for the density of states versus  $r_s$  evaluated at different temperatures are plotted in Fig. 9. Two different types of a behavior of  $N(r_s)$  can be distinguished. Consider first the lowest of the four curves, corresponding to  $\tau = T/\epsilon_F^0 = 10^{-3}$ . This curve shows a monotonic increase of the density of states, with a change of slope near the QCP, behavior which can be understood as follows. Below the QCP, i.e. at  $r_s < r_s^\infty$ , the density of states  $N(T, r_s)$  is proportional to the effective mass  $M^*(T, r_s)$  which, in the vicinity of the QCP, behaves as<sup>21</sup>

$$\frac{M^*(r_s, T)}{M} \sim \frac{1}{\kappa D(r_s) + \nu \tau^{2/3}}. \quad (28)$$

Here, the positive constant  $D(r_s) \propto 1 - r_s/r_s^\infty$  is the coefficient of the linear term (in  $p - p_F$ ) of the formula (13) for  $\epsilon(p)$ , which provides a good approximation to the quasiparticle spectrum. In Eq. (28),  $\nu = (9\lambda/4)^{1/3}$  is determined by the  $r_s$ -independent parameter  $\lambda$  controlling the cubic term in Eq. (13) (see Ref. 21), while  $\kappa$  is a constant of order one. Beyond the QCP, a fermion condensate is present at  $T/\epsilon_F^0 = 10^{-3}$ . The behavior of  $N(r_s, T)$  in the state with a FC results from the interplay of two contributions, as described by Eq. (22). The first contribution, associated with the FC, behaves like  $\eta\tau^{-1} \propto |D(r_s)|^{1/2}\tau^{-1}$ , while the second, coming from re-

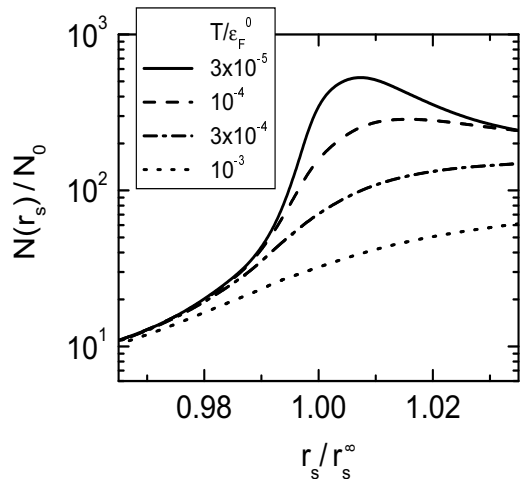


FIG. 9: Density of states  $N(r_s)$  in units of  $N_0$  for the 2D electron gas at four values of temperature  $T$  in units of  $\epsilon_F^0$ .

gions adjacent to the FC domain, is proportional to  $\tau^{-2/3}$  and independent of  $r_s$ .

We turn now to the uppermost curve in Fig. 9, corresponding to  $\tau = 3 \times 10^{-5}$ . Below the QCP, the behavior of this curve can also be understood in terms of Eq. (28). Beyond the QCP, the bubble rearrangement is favored by the low temperature, and the resulting FL behavior of the density of states can be again described by Eq. (28), with all three sheets of the Fermi surface taking part and making the coefficient  $\kappa$  considerably larger than unity.

An essential message of Fig. 9 is that at sufficiently low temperature, the effective mass of the 2D electron gas extracted from an analysis of its thermodynamic properties should *decrease* beyond the QCP.

## V. QUASIPARTICLE PHASE DIAGRAM

The information we have gained on the behavior of quasiparticle degrees of freedom of the 2D electron gas near the quantum critical point may be integrated into a quasiparticle phase diagram. We do this with the caveat that our treatment has not taken into account the feedback of the modification of single-particle degrees of freedom on any pertinent collective modes. Accordingly, what we obtain is only a “quasiparticle sketch” of the real phase diagram of the system.

Phase diagrams of other strongly correlated systems are customarily drawn in a  $T - x$  plane, where  $x$  is some external parameters, notably pressure, doping, or magnetic field. Instead of these, we have considered variations of the spacing parameter  $r_s$  measuring the extent to which the system is rarefied. Thus, in Fig. 10 the phase diagram of the 2D electron gas is drawn in  $(T, x)$  variables, with  $x = 1 - r_s/r_s^\infty$ . On the top axis of the plot, we show also the coefficient  $D(x) \propto x$  of the linear term in Eq. (13) for the quasiparticle spectrum. The

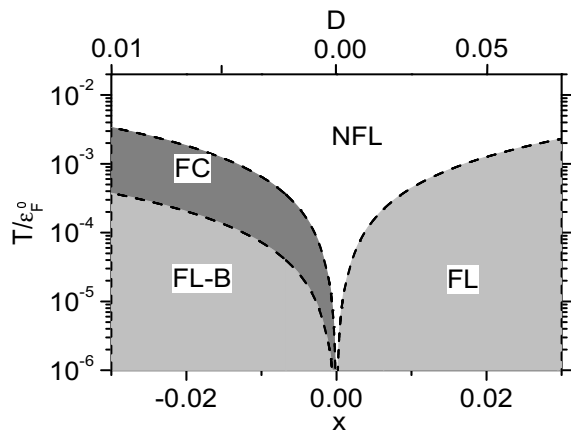


FIG. 10: Quasiparticle phase diagram of the 2D electron gas in  $(T, x)$  variables with  $x = 1 - r_s/r_s^\infty$ . The dashed curves show crossovers between the usual Fermi liquid (FL), the Fermi liquid with bubble (FL-B), the fermion condensate (FC) state, and the non-Fermi-liquid (NFL) phase with critical index  $\alpha \simeq 0.6$ . The parameter  $D(x)$  is indicated on the top axis.

latter parameter is positive below the QCP and negative above; its vanishing at the QCP reflects the emergence of the horizontal inflection point in the quasiparticle energy. Beyond the QCP, the negative sign of  $D(r_s)$  corresponds to three roots of the equation  $\epsilon(p) = 0$ , and the presence of a bubble in the quasiparticle momentum distribution.

Inspecting the phase diagram presented in Fig. 10, we start from the side to the right of  $x_\infty$ , i.e., below the QCP, where  $D(r_s) > 0$ . Here the low-temperature region of the diagram is occupied by an ordinary Landau Fermi liquid. The foregoing analysis tells us that at a temperature around  $T^*$ , a crossover occurs from the FL regime to a universal NFL domain that occupies the upper part of the diagram. The dependence  $T^*(D)$  can be estimated using Eq. (28). As a function of  $T$ , the behavior of this expression changes at a temperature for which  $\nu\tau^{2/3} \sim D$ . Thus we estimate that the temperature of the crossover to the NFL behavior in the domain  $x > 0$  goes like

$$T^*(D > 0) \sim \nu^{-3/2} |D|^{3/2} \varepsilon_F^0. \quad (29)$$

This temperature is traced by the dashed line in the right side of the phase diagram of Fig. 10, separating the light gray FL region from the white NFL region.

Now consider the left side of the phase diagram lying *beyond* the QCP, where  $D(x) < 0$  and two crossovers occur. Under increasing temperature there is first a crossover from the FL state having a bubble (FL-B) to the FC state. An estimate of the temperature  $T_0$  of this crossover was made in Sec. III, with the result  $\tau_0 \sim |D|\eta$ . The dependence of  $\eta$  on  $D$  can be easily found by solving the equation  $\epsilon(p) = 0$ , which identifies the boundaries of the region in which the Landau quasiparticle distribution is altered. For the spectrum as represented by Eq. (13),

this equation has the explicit form

$$D\eta + \nu^3\eta^3/9 = 0, \quad (30)$$

yielding

$$\eta = 3\nu^{-3/2}|D|^{1/2}. \quad (31)$$

Incorporating this dependence into  $\tau_0 \sim |D|\eta$ , we obtain

$$T_0(D < 0) \sim 3\nu^{-3/2}|D|^{3/2} \varepsilon_F^0. \quad (32)$$

The crossover in question is indicated in Fig. 10 by the curve in the left part of the phase diagram separating the light-gray FL-B regime from the gray region corresponding to the FC state.

The second crossover, from the FC regime to the universal NFL regime with critical index 0.6, occurs as the temperature increases up to the value  $T^*(D < 0)$  at which the FC contribution to thermodynamic characteristics of the system and that of regions adjacent to the FC territory become comparable. For example, the FC contribution to the density of states has been estimated in Sec. IV as  $\eta\tau^{-1}$ , and that from adjacent regions, as  $\nu^{-1}\tau^{-2/3}$ . This implies that  $\tau^*(D < 0) \sim \nu^3\eta^3$  and hence

$$T^*(D < 0) \sim 27\nu^{-3/2}|D|^{3/2} \varepsilon_F^0. \quad (33)$$

The resulting dependence of  $T^*(D < 0)$  on  $x$  is shown by the upper curve in the left part of the phase diagram, which separates the FC region from the NFL region.

As mentioned at the beginning of this section, the phase diagram we have generated is a semi-finished product. The next step in building a complete phase diagram of the 2D electron gas is to characterize the feedback from rearrangement of the single-particle degrees of freedom on the collective modes. It is expected that one of the Pomeranchuk stability conditions is eventually violated, leading to collapse of the corresponding collective mode. Preliminary analysis indicates that this violation may be due to unusual behavior of the quasiparticle polarization operator beyond the QCP. Future work will aim at determining which channel of instability is the first to appear.

## VI. CONCLUSIONS

We have studied low-temperature properties of the 2D electron gas at densities close to the point  $\rho_\infty$  of divergence of the quasiparticle effective mass. A number of significant results have been obtained by means of a microscopic approach based on fundamental relations of the Landau Fermi-liquid theory and an approximate evaluation of the quasiparticle interaction function.

For  $r_s < r_s^\infty$ , i.e., for values of the dilution parameter below the point of divergence of the effective mass, we find that the temperature  $T^*$  up to which the 2D electron gas continues to exhibit FL thermodynamic properties, decreases with increasing  $r_s$  and vanishes as  $r_s$



approaches  $r_s^\infty$ . At  $T \sim T^*$ , a crossover occurs to universal NFL behavior of thermodynamic properties: the density of states  $N(T)$ , the spin susceptibility  $\chi(T)$ , and the ratio  $C(T)/T$  of the specific heat to temperature scale universally as  $T^{-\alpha}$  with critical index  $\alpha \simeq 0.6$ . This finding is consistent with predictions of the inflection-point model of the quantum critical point (QCP).<sup>21</sup>

We have evaluated the spectrum  $\epsilon(p)$  and the momentum distribution  $n(p)$  of quasiparticles beyond the QCP, i.e. at  $r_s > r_s^\infty$ . In this regime, the single-particle degrees of freedom are altered, more or less profoundly, relative to the standard FL picture. At very low temperatures, the new quasiparticle momentum distribution is multi-connected. An empty ring appears in the occupied Fermi circle, as the self-consistent quasiparticle spectrum  $\epsilon(p)$  acquires a cubic-like shape with three zeroes at three boundary momenta. This state, however, possesses the usual Fermi liquid thermodynamic properties, in that  $N(T)$  is temperature independent, as are  $\chi(T)$  and the ratio  $C(T)/T$ . Moreover, the Sommerfield-Wilson ratio is unity, as it should be in a FL state.

When the temperature rises to a certain value  $T_0$ , a crossover to a state having a fermion condensate is found to occur. This more radical rearrangement of the single-particle degrees of freedom is distinguished by *fractional* occupation of momentum states, hence essential departure from the conventional Landau Fermi-liquid picture, over a finite range of momenta where the fermion condensate resides. The momentum distribution  $n_*(p, T > T_0)$  in this domain, as well as the ratio  $\epsilon(p, T)/T$ , proves to be independent of temperature; the spectrum  $\epsilon(p, T)$  itself, being proportional to  $T$ , proves to be almost flat. The temperature dependence of the density of states  $N(T)$ , and likewise for the spin susceptibility  $\chi(T)$ , is determined by an interplay of a pure FC term proportional to  $T^{-1}$  and a NFL term proportional to  $T^{-2/3}$ . The temperature dependence of the entropy is weak, while the specific heat decreases sharply and the Sommerfield-Wilson ratio jumps up to about 7. With further increase of temperature, a second crossover is found, going from the FC state to the state with universal NFL behavior.

Assembling results from the analysis of thermodynamic properties, we have sketched a quasiparticle phase diagram of the dilute 2D electron gas in the immediate vicinity of the QCP. There are four regions in this diagram: (i) a conventional one corresponding the FL behavior of ordinary Landau quasiparticles, (ii) the region associated with the multi-connected quasiparticle distribution where FL temperature behavior persists, (iii) the domain created by the FC rearrangement, and (iv) the regime of universal NFL behavior.

Also of interest is our finding that at a fixed temperature for which the multi-connected quasiparticle distribution is favored, there is an enormous enhancement of the effective mass  $M^*$  as  $r_s$  increases to the QCP, but no true divergence. Moreover, beyond  $r_s^\infty$ , this enhancement is followed by a decrease of  $M^*$ . At temperatures

for which the FC state is favored, the rate of growth of the effective mass decreases with increasing  $r_s$  beyond the QCP.

New experiments using ultraclean Si-MOS samples could clarify the nature of the QCP in 2D electronic systems inhabiting these structures.

The authors are grateful to V. T. Dolgoplov, L. A. Maksimov, Yu. M. Kagan, A. A. Shashkin, and G. E. Volovik for valuable discussions. This research was supported by Grant No. NS-8756.2006.2 from the Russian Ministry of Education and Science. MVZ thanks INFN (Sezione di Catania) for hospitality during his stay in Catania.

## APPENDIX

In this appendix we describe the scheme adopted for evaluation of the quasiparticle interaction function as expressed in Eq. (8). A microscopic functional approach to this problem begins with the connection

$$\chi(q, \omega) = \frac{\chi_0(q, \omega)}{1 - R(q, \omega)\chi_0(q, \omega)} \quad (34)$$

of the linear response function  $\chi(q, \omega)$  entering the integrand in the r.h.s. of Eq. (8) to the response function  $\chi_0(q, \omega)$  of the noninteracting gas, through the effective interaction  $R(q, \omega)$ . Accordingly, variation of the response function  $\chi(q, \omega)$  affects both the function  $\chi_0(q, \omega)$  and the effective interaction  $R(q, \omega)$ :

$$\begin{aligned} \frac{\delta^2 \chi(q, \omega)}{\delta n(\mathbf{p}) \delta n(\mathbf{p}')} &= \frac{\delta^2 \chi_0(q, \omega)}{\delta n(\mathbf{p}) \delta n(\mathbf{p}')} \varphi^2(q, \omega) \\ + 2 \varphi^3(q, \omega) R(q, \omega) &\frac{\delta \chi_0(q, \omega)}{\delta n(\mathbf{p})} \frac{\delta \chi_0(q, \omega)}{\delta n(\mathbf{p}')} \\ + \text{terms containing} &\frac{\delta R(q, \omega)}{\delta n(\mathbf{p})}, \end{aligned} \quad (35)$$

where  $\varphi(q, \omega) = [1 - R(q, \omega)\chi_0(q, \omega)]^{-1}$ .

The analysis performed in Ref. 20 indicates that the shape of the effective interaction has a rather smooth dependence on  $r_s$ . For this reason, the terms containing the variational derivative  $\delta R(q, \omega)/\delta n(\mathbf{p})$  serve only to produce a slight renormalization of the chemical potential, without contributing significantly to the shape of the spectrum. By the same token, these terms are also neglected in the present treatment.

We consider first the contribution  $f^{(1)}(\mathbf{p}, \mathbf{p}')$  to the interaction function resulting from the product of first variational derivatives of the function  $\chi_0(q, \omega)$ , namely

$$\begin{aligned}
f^{(1)}(\mathbf{p}, \mathbf{p}') = & -2 \int_0^{e^2} de^2 \int \frac{d^2q}{2\pi q} R(q, \omega) \left[ (1 - n_{\text{FL}}(\mathbf{p}-\mathbf{q})) (1 - n_{\text{FL}}(\mathbf{p}'-\mathbf{q})) \delta(\epsilon_{\mathbf{p}}^0 - \epsilon_{\mathbf{p}'}^0 - \epsilon_{\mathbf{p}-\mathbf{q}}^0 + \epsilon_{\mathbf{p}'-\mathbf{q}}^0) \varphi^3(q, \epsilon_{\mathbf{p}}^0 - \epsilon_{\mathbf{p}-\mathbf{q}}^0) - \right. \\
& - \frac{(1 - n_{\text{FL}}(\mathbf{p}-\mathbf{q})) (\epsilon_{\mathbf{p}}^0 - \epsilon_{\mathbf{p}-\mathbf{q}}^0)}{(\epsilon_{\mathbf{p}}^0 - \epsilon_{\mathbf{p}-\mathbf{q}}^0)^2 - (\epsilon_{\mathbf{p}'}^0 - \epsilon_{\mathbf{p}'-\mathbf{q}}^0)^2} \varphi^3(q, \epsilon_{\mathbf{p}'}^0 - \epsilon_{\mathbf{p}'-\mathbf{q}}^0) - \frac{(1 - n_{\text{FL}}(\mathbf{p}'-\mathbf{q})) (\epsilon_{\mathbf{p}'}^0 - \epsilon_{\mathbf{p}'-\mathbf{q}}^0)}{(\epsilon_{\mathbf{p}'}^0 - \epsilon_{\mathbf{p}'-\mathbf{q}}^0)^2 - (\epsilon_{\mathbf{p}}^0 - \epsilon_{\mathbf{p}-\mathbf{q}}^0)^2} \varphi^3(q, \epsilon_{\mathbf{p}}^0 - \epsilon_{\mathbf{p}-\mathbf{q}}^0) + \\
& \left. + \int_{-\infty}^{\infty} \frac{dw}{2\pi} \frac{(\epsilon_{\mathbf{p}}^0 - \epsilon_{\mathbf{p}-\mathbf{q}}^0) (\epsilon_{\mathbf{p}'}^0 - \epsilon_{\mathbf{p}'-\mathbf{q}}^0)}{[(\epsilon_{\mathbf{p}}^0 - \epsilon_{\mathbf{p}-\mathbf{q}}^0)^2 + w^2] [(\epsilon_{\mathbf{p}'}^0 - \epsilon_{\mathbf{p}'-\mathbf{q}}^0)^2 + w^2]} \varphi^3(q, iw) \right]. \quad (36)
\end{aligned}$$

Following the strategy discussed in Section II, we assume that both of the momenta  $\mathbf{p}$  and  $\mathbf{p}'$  are located near the Fermi surface. We also assume both of them to be larger than  $p_F$ , as is conventionally done in other problems of this kind. Thus, we deal with the function  $f^{(1)}(x) = f^{(1)}(p_F, p_F, x)$ , where  $x = \cos(\mathbf{p}, \mathbf{p}')$ , and we are interested in the region  $x \sim -1$  that corresponds to backward scattering and provides the main contribution to the shape of the spectrum near the Fermi surface. It should be kept in mind that within the diluteness regime under consideration, i.e.,  $r_s \sim r_s^\infty$ , the function  $\varphi(q, 0)$  possesses a sharp maximum at  $q \simeq 2p_F$ , such that the dominant contribution to the integral in Eq. (36) comes from the region where  $q \sim 2p_F$ . Assuming  $\epsilon_{\mathbf{p}}^0 = \epsilon_{\mathbf{p}'}^0 = 0$ , we note that the first term of the integrand of Eq. (36) contains the delta-function  $\delta(\epsilon_{\mathbf{p}-\mathbf{q}}^0 - \epsilon_{\mathbf{p}'-\mathbf{q}}^0)$ . For  $x \sim -1$ , the condition of equality of the energies  $\epsilon_{\mathbf{p}-\mathbf{q}}^0$  and  $\epsilon_{\mathbf{p}'-\mathbf{q}}^0$  suppresses the integral over angles of the vector  $\mathbf{q}$ , since it receives contributions only from directions of  $\mathbf{q}$  tangent to the Fermi surface at the points  $\mathbf{p}$  and  $\mathbf{p}'$ . The first term of the integrand in Eq. (36) yields appreciable contributions to  $f^{(1)}(x)$  only at  $x \sim 1$ , noting that in this case all directions of  $\mathbf{q}$  carry similar weight. The second and third terms of the integrand contain expressions

$$\frac{\epsilon_{\mathbf{p}-\mathbf{q}}^0}{(\epsilon_{\mathbf{p}-\mathbf{q}}^0)^2 - (\epsilon_{\mathbf{p}'-\mathbf{q}}^0)^2} \quad \text{and} \quad \frac{\epsilon_{\mathbf{p}'-\mathbf{q}}^0}{(\epsilon_{\mathbf{p}-\mathbf{q}}^0)^2 - (\epsilon_{\mathbf{p}'-\mathbf{q}}^0)^2},$$

respectively, thus implying that their contributions peak at  $\epsilon_{\mathbf{p}-\mathbf{q}}^0 \simeq \epsilon_{\mathbf{p}'-\mathbf{q}}^0$ . The same considerations as for the first term show that neither of these terms contributes noticeably to  $f^{(1)}(x)$  at  $x \sim -1$ . In the fourth term, the region  $w \lesssim 1$  dominates the integration over the variable  $w$ . When evaluated within the approximation  $R(q, w \lesssim 1) \simeq R(q, 0)$  (which overestimates the integral), the fourth term produces a contribution

$$\tilde{f}^{(1)}(x) \sim -2 \int_0^{e^2} de^2 \int \frac{d^2q}{2\pi q} \frac{R(q, 0) \varphi^3(q, 0)}{\epsilon_{\mathbf{p}_F-\mathbf{q}}^0 + \epsilon_{\mathbf{p}'_F-\mathbf{q}}^0} \quad (37)$$

to the interaction function. An estimate of the corre-

sponding contribution to  $f(x \sim -1)$ , made by replacement of the denominator in Eq. (37) by its approximate value  $q^2/M$ , indicates that the effect is rather small, namely about 10 – 15% at  $r_s \sim 7$ . This contribution has not been neglected, but instead is evaluated approximately.

We turn now to evaluation of the main term in the interaction function, denoted  $f^{(2)}(\mathbf{p}, \mathbf{p}')$ , containing the second variational derivative of the response  $\chi_0(q, \omega)$ . This derivative is easily evaluated as

$$\frac{1}{2} \frac{\delta^2 \chi(q, \omega)}{2 \delta n(\mathbf{p}) \delta n(\mathbf{p}')} = (2\pi)^2 \delta(\epsilon_{\mathbf{p}}^0 - \epsilon_{\mathbf{p}'}^0 - \omega) \delta(\mathbf{q} - \mathbf{p} + \mathbf{p}'), \quad (38)$$

and we then obtain

$$f^{(2)}(\mathbf{p}, \mathbf{p}') = - \int_0^{e^2} de^2 \frac{2\pi}{|\mathbf{p} - \mathbf{p}'|} \varphi^2(\mathbf{p} - \mathbf{p}', \epsilon_{\mathbf{p}}^0 - \epsilon_{\mathbf{p}'}^0). \quad (39)$$

For momenta  $\mathbf{p}$  and  $\mathbf{p}'$  lying at the Fermi surface, Eq. (39) reduces to the expression

$$f^{(2)}(q) = - \frac{2\pi}{q} \int_0^{e^2} de^2 \varphi^2(q, 0), \quad (40)$$

the integral over  $e^2$  being evaluated numerically.

The interaction function  $f^{(2)}(q)$  calculated for the 2D electron gas at  $r_s = 6, 7, \text{ and } 8$  is displayed in Fig. 11. The absolute value of this function is seen to possess a strongly pronounced maximum at  $q = q_c \simeq 2p_F$ , which increases with increasing  $r_s$ . The peak and its enhancement with increasing  $r_s$  are related to the proximity of the system to an instability against spontaneous appearance of charge-density waves (CDW) with wave vector  $q_c$  (see Refs. 20,26,27,28). This situation is known to be responsible for divergence of the effective mass.<sup>29,30</sup> In this regard, it is worth noting that the *negative* sign obtained for the quasiparticle interaction function  $f(q \sim 2p_F)$  provides the correct positive sign of the first harmonic,

$$F_1 = N_0 \int_{-1}^1 f(x) \frac{x}{\sqrt{1-x^2}} \frac{dx}{2\pi}, \quad (41)$$

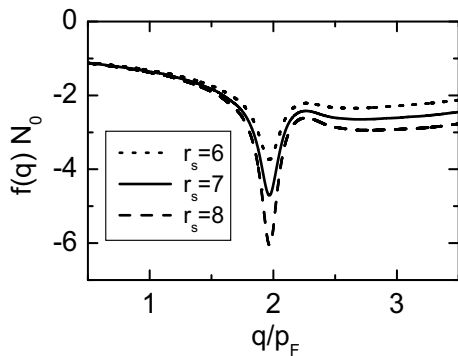


FIG. 11: Quasiparticle interaction function, calculated within the microscopic functional approach for the 2D electron gas and plotted as  $f(q)N_0$  at three values of the diluteness parameter  $r_s$ .

which equals 1 at the QCP. At the same time, the *negative* sign of the quasiparticle amplitude does not support the idea that the quasiparticle weight  $Z$  vanishes near a CDW instability. The latter eventuality is possible only in case the quasiparticle amplitude, divergent at  $q \sim 2p_F$ , has a *positive* sign, as erroneously assumed in Ref. 16 in considering enhancement of the amplitude in the vicinity of such an instability.

- 
- <sup>1</sup> F. F. Fang and P. J. Stiles, Phys. Rev. **174**, 823 (1968).  
<sup>2</sup> A. A. Shashkin, S. V. Kravchenko, V. T. Dolgoplov *et al.*, Phys. Rev. B **66**, 073303 (2002).  
<sup>3</sup> V. M. Pudalov, M. E. Gershenson, H. Kojima, *et al.*, Phys. Rev. Lett. **88**, 196404 (2002).  
<sup>4</sup> A. Casey, H. Patel, J. Nyeki, B. P. Cowan, and J. Saunders, Phys. Rev. Lett. **90**, 115301 (2003).  
<sup>5</sup> C. Bäuerle, Yu. M. Bunkov, A. S. Chen, S. N. Fisher, and H. Godfrin, J. Low Temp. **110**, 333 (1998).  
<sup>6</sup> C. Bäuerle, J. Bossy, Yu. M. Bunkov, A. S. Chen, H. Godfrin, and M. Roger, J. Low Temp. Phys. **110**, 345 (1998).  
<sup>7</sup> A. Schröder, G. Aeppli, R. Coldea *et al.*, Nature **407**, 351 (2000).  
<sup>8</sup> G. R. Stewart, Rev. Mod. Phys. **73**, 787 (2001).  
<sup>9</sup> D. Takahashi, S. Abe, H. Mizuno *et al.*, Phys. Rev. B **67**, 180407 (2003).  
<sup>10</sup> R. Küchler, N. Oeschler, P. Gegenwart *et al.*, Phys. Rev. Lett. **91**, 066405 (2002).  
<sup>11</sup> J. Custers, P. Gegenwart, H. Wilhelm *et al.*, Nature **424**, 524 (2003).  
<sup>12</sup> P. Gegenwart *et al.*, Acta Phys. Pol. **B34**, 323 (2003).  
<sup>13</sup> P. Coleman, C. Pépin, Q. Si, and R. Ramazashvili J. Phys.: Condens. Matter **13**, R723 (2001).  
<sup>14</sup> J. A. Hertz, Phys. Rev. B **14**, 1165 (1976).  
<sup>15</sup> A. J. Millis, Phys. Rev. B **48**, 7153 (1993).  
<sup>16</sup> A. V. Chubukov, V. M. Galitski, and V. M. Yakovenko, Phys. Rev. Lett. **94**, 046404 (2005).  
<sup>17</sup> A. A. Shashkin, M. Rahimi, S. Anissimova *et al.*, Phys. Rev. Lett. **91**, 046403 (2003).  
<sup>18</sup> V. R. Shaginyan, Solid State Commun. **55**, 9 (1985).  
<sup>19</sup> V. A. Khodel, V. V. Khodel, and V. R. Shaginyan, Phys. Rep. **249**, 1 (1994).  
<sup>20</sup> V. V. Borisov and M. V. Zverev, JETP Letters **81**, 503 (2005).  
<sup>21</sup> J. W. Clark, V. A. Khodel, and M. V. Zverev, Phys. Rev. B **71**, 012401 (2005).  
<sup>22</sup> T. Okamoto, M. Ooya, K. Hosoya, and S. Kawaji, Phys. Rev. B **69**, 041202 (2004).  
<sup>23</sup> J. Boronat, J. Casulleras, V. Grau, E. Krotscheck, and J. Springer, Phys. Rev. Lett. **91**, 085302 (2003).  
<sup>24</sup> J. W. Clark and E. Feenberg, Phys. Rev. **113**, 388 (1959).  
<sup>25</sup> E. Feenberg, *Theory of Quantum Fluids* (Academic Press, New York, 1969).  
<sup>26</sup> D. Pines, P. Nozières, *Theory of quantum liquids*, Benjamin, New York, 1966.  
<sup>27</sup> L. Swierkowski, D. Neilson, and J. Szymanski, Phys. Rev. Lett. **67**, 240 (1991).  
<sup>28</sup> A. Gold and L. Calmels, Phys. Rev. B **48**, 11622 (1993).  
<sup>29</sup> V. A. Khodel, V. R. Shaginyan, and M. V. Zverev, JETP Letters **65**, 253 (1997).  
<sup>30</sup> V. M. Galitski and V. A. Khodel, cond-mat/0308203.  
<sup>31</sup> H. Fröhlich, Phys. Rev. **79**, 845 (1950).  
<sup>32</sup> I. M. Lifshitz, Sov. Phys. JETP **11**, 1130 (1960).  
<sup>33</sup> M. V. Zverev and M. Baldo, J. Phys.: Condens. Matter **11**, 2059 (1999).  
<sup>34</sup> P. Nozières, J. Phys. I France **2**, 443 (1992).  
<sup>35</sup> J. M. Kosterlitz and D. J. Thouless, J. Phys. C **6**, 1181 (1973).  
<sup>36</sup> M. Baldo, V. V. Borisov, J. W. Clark, V. A. Khodel, and M. V. Zverev, J. Phys.: Cond. Matter, **16**, 6431 (2004).  
<sup>37</sup> P. Gegenwart *et al.*, Phys. Rev. Lett. **39**, 076402 (2005).  
<sup>38</sup> V. A. Khodel, M. V. Zverev, and J. W. Clark, JETP Letters **81**, 315 (2005).  
<sup>39</sup> B. Doniach and S. Engelsberg, Phys. Rev. Lett. **17**, 750 (1966).  
<sup>40</sup> W. F. Brinkman and T. M. Rice, Phys. Rev. B **2**, 4302 (1970).  
<sup>41</sup> A. M. Dyugaev, Sov. Phys. JETP **43**, 1247 (1976).  
<sup>42</sup> A. B. Migdal, *Theory of Finite Fermi Systems and Applications to Atomic Nuclei*, New York: Wiley, 1967.